Journal of Science and Transport Technology
Journal homepage: https://jstt.vn/index.php/en

Experimental investigation of mechanical properties of coral concrete under cyclic compression

Viet Chinh Mai[1,*], Duc Tiep Pham[1], Quoc Anh Vu[2], Trung Hieu Tran[2], Trung Dinh Quang[1]

[1]Institute of Construction Technology, Le Quy Don Technical University, Hanoi, Vietnam

[2]Hanoi Architectural University, Hanoi, Vietnam

Article info
Type of article:
Original research paper

DOI:
https://doi.org/10.58845/jstt.utt.2025.en.5.4.63-86

***Corresponding author:**
Email address:
maivietchinh@lqdtu.edu.vn

Received: 04/08/2025
Received in Revised Form: 02/10/2025
Accepted: 07/11/2025

Abstract: The increasing depletion of terrestrial resources and the growing demand for offshore infrastructure have heightened the need for sustainable construction solutions utilizing locally available marine materials. Coral concrete, composed of coral coarse aggregates, coral sand, and seawater, emerges as a promising alternative to conventional concrete, particularly for construction on remote islands and reefs. This study presents a pioneering experimental examination of the cyclic compression behavior of coral concrete, thereby addressing a research gap in existing literature. It investigates the mechanical behavior of coral concrete under cyclic compression loading, with a focus on its compressive strength, stress-strain response, stiffness degradation. The results indicate that coral concrete exhibits markedly different mechanical responses when subjected to cyclic loading, showing up to a 20% reduction in average compressive strength and a maximum degradation of 23.1% in secant elastic modulus compared to specimens not exposed to cyclic loading. The initiation and propagation of microcracks occurred rapidly, primarily along the aggregate-paste interfaces due to the porous and fragile nature of coral aggregates. These findings not only underline the vulnerability of coral concrete to fatigue-related damage but also provide practical insights for the design and optimization of offshore and island infrastructures.

Keywords: Coral concrete; coral sand; cyclic compression; mechanical properties; marine engineering; sustainable construction.

1. Introduction

The continuous depletion of terrestrial resources, coupled with the escalating demand for offshore infrastructure, has underscored the importance of sustainable construction solutions for remote islands and reefs. The strategic significance of these structures extends beyond territorial integrity and sovereignty, offering considerable military and economic value [1, 2]. However, the scarcity of traditional construction materials on offshore islands poses a significant challenge, resulting in increased transportation costs and logistical complexities [3-5]. To address this issue, coral concrete, composed of locally abundant coral aggregates and coral sand, has emerged as a viable alternative [6-8].

Regarding the investigation of the mechanical properties of coral concrete and its

applications in construction, numerous studies have been conducted. Study of Da et al. [9] utilized a combination of experimental tests and numerical simulations to analyze the mechanical properties of coral aggregate seawater concrete, focusing on compressive strength, splitting tensile strength, and the stress-strain curve for strength grades ranging from C30 to C55. The proposed numerical model demonstrated improved accuracy, reducing prediction errors to 2.5%-5.7% compared to experimental results. However, the study lacked a comprehensive analysis of long-term durability and corrosion resistance of coral concrete in harsh marine environments. Wang et al. [1] investigated the mechanical properties and microstructure of sea sand coral concrete (SSCC) through compressive and flexural tests, focusing on the stress-strain behavior and interfacial transition zone. A two-stage uniaxial compression constitutive model was proposed to predict SSCC's behavior, revealing that the material exhibited rapid damage with significant variations in the descending section of the stress-strain curve. While the study highlighted the superior binding of coral aggregate to the cement matrix, it failed to account for the effects of environmental factors such as high salinity and temperature fluctuations on SSCC performance. In the work conducted by Huang et al., the influence of various mix components, including sea sand, seawater, fly ash, and cement, on the mechanical properties of coral concrete (CC) was studied. The results demonstrated that seawater improved the elastic modulus and strength of CC, whereas sea sand negatively impacted performance. A numerical expression for the stress-strain curve was proposed to account for these effects. However, the study did not assess the long-term mechanical properties of CC, nor did it evaluate the potential benefits of fiber reinforcement or advanced admixtures in enhancing CC's ductility and durability [10]. Ma et al. [11] explored the behavior of coral concrete under dynamic loading, analyzing its strain rate sensitivity, energy dissipation, and fractal dimensions. The findings revealed that coral concrete exhibited high-early strength and brittle post-peak behavior, with the dynamic increase factor (DIF) ranging from 1.73 to 2.56. The fracture planes penetrated the coral aggregates rather than the mortar interface, distinguishing it from conventional concrete. Study of Wang et al. [12] focused on the stress-strain behavior of coral fly ash-slag alkali-activated concrete (CAAC) using monotonic loading tests to derive elastic modulus, Poisson's ratio, and a piecewise constitutive model. The results highlighted similarities between CAAC, lightweight aggregate concrete, and conventional coral concrete, with CAAC showing improved strength and toughness. Despite these findings, the research lacked practical application data for large-scale engineering projects and did not address the long-term corrosion resistance or durability of CAAC in marine environments. Based on the conducted research, it is evident that coral concrete leverages the unique properties of coral aggregates, including their lightweight and porous nature, to provide a cost-effective and environmentally friendly building material. Despite these advantages, coral concrete exhibits higher brittleness and lower strength compared to ordinary concrete, necessitating further research to enhance its mechanical performance [11, 13]. Recent studies have highlighted the potential of fiber reinforcement, such as sisal and polypropylene fibers, to improve the ductility, energy dissipation, and durability of coral concrete [2, 13, 14].

Cyclic compression, a frequently encountered stress condition in marine environments, imposes additional mechanical challenges on coral concrete structures, particularly those situated on offshore islands and artificial reefs. These conditions, often caused by repeated wave action, tidal fluctuations, and dynamic loading from marine operations, can accelerate material degradation and compromise structural integrity over time. The unique mechanical behavior of coral concrete under such

cyclic loading scenarios including variations in compressive strength, stiffness degradation, and progressive damage accumulation remains insufficiently investigated in current literature. Bridging this knowledge gap is essential for optimizing both the structural performance and long-term durability of coral concrete elements in demanding offshore environments. This study aims to investigate the mechanical properties of coral concrete under cyclic compression, with particular emphasis on analyzing its stress–strain response, modulus evolution, and damage mechanisms. The outcomes of this research are expected to provide valuable insights into the fatigue behavior of coral concrete, contributing to more effective material design, reduced construction costs, improved resource utilization, and enhanced resilience of coastal and offshore infrastructure systems.

2. Materials and Methods

The coral concrete utilized in the present study is composed of Portland cement PCB 40, coral coarse aggregates, coral sand, and seawater.

2.1. Materials and properties

PCB40, a type of cement widely recognized for its high quality stability, is readily available in Vietnam. The experimental results outlining its physical and mechanical properties are presented in Table 1 [15, 16].

Table 1. Physical and mechanical properties of PCB40 cement

No.	Parameter	Unit	Value
1	Density	g/cm^3	3.0
2	Fineness (residue on a 90 μm sieve)	%	5.8
3	Standard water consistency	%	29
4	Volume stability	mm	5.2
5	Compressive strength - At 3 days	MPa	21
	- At 28 days	MPa	43.4

Table 2 provides the chemical composition of seawater collected from offshore islands in Vietnam [17, 18]. The seawater exhibits a pH value of 6.8 and contains various dissolved ions, including chloride (15.3 g/l), calcium (0.3 g/l), magnesium (1.1 g/l), sulfate (2.4 g/l), potassium (0.35 g/l), and sodium (8.5 g/l).

Table 2. Chemical composition of seawater

PH	Cl- g/l	Ca+ g/l	Mg+ g/l	SO42- g/l	K+ g/l	Na+ g/l
6.8	15.3	0.3	1.1	2.4	0.35	8.5

The coral coarse aggregates used in this study were obtained from offshore islands in Vietnam, crushed, and screened to achieve a grain size of 1×2 cm. According to ASTM C33/C33M-2018 [19], the experimental results outlining its physical and mechanical properties that are provided in Table 3. The cumulative sieve residue percentages indicate the proportion of particles retained on sieves with sizes of 5, 10, and 20 mm, showing values of 98%, 95%, and 4%, respectively. The water absorption of the aggregates is measured at 3.92%, while the porosity density is recorded at 980 kg/m^3.

Table 3. Physical properties of coarse aggregates

Index property	Unit	Value		
Sieve size	mm	5	10	20
Cumulative sieve residue	%	98	95	4
Water absorption	%	3.92		
Porosity density	kg/m^3	980		
Cylinder compression strength	%	46		
Elongated particle ratio	%	19.6		
Dust and clay ratio	%	0.41		

The experimental results indicate that coral exhibits high compressive strength, greater water absorption compared to conventional crushed stone, a rough surface with numerous open pores, and a sharp angular morphology, with some particles displaying a rodlike shape. The shape and surface characteristics of coral are illustrated in Fig. 1.

The fine aggregate is coral sand extracted from the offshore island, sourced from the same location as the coral coarse aggregate. Observations indicate that the coral sand possesses a rough, angular texture. The physical

properties of the coral sand are presented in Table 4.

Fig. 1. Coral coarse aggregates (1x2mm) from the Vietnam offshore island

Table 4. Physical properties of coral sand

Index property	Unit	Value					
Sieve size	mm	5	2.5	1.25	0.63	0.315	0.14
Cumulative sieve residue	%	13.5	31.4	48	66.9	84.4	94.6
Water absorption	%	14.4					
Dust and clay ratio	%	1					
Porosity density	kg/m^3	1120					
Fineness modulus	//	2.2					

2.2. Mix Proportion

Due to the irregular geometry, rough surface texture, and inherently high porosity of coral aggregates, the mix design of coral concrete does not conform to conventional concrete design principles. Instead, it adopts key concepts from the design philosophy of reactive powder concrete, which emphasizes dense packing, high cementitious content. To compensate for the weaker mechanical properties and absorptive characteristics of coral aggregate, a higher proportion of cementitious material is incorporated, along with an increased volume of fine aggregates (coral sand), and the bulk volume method is employed to ensure proper packing density and cohesion within the matrix [20-22]. In this study, the coral concrete is formulated to target a strength grade of C30, with a selected water-to-cement ratio (W/C) of 0.62. The complete mix composition, including quantities of cement, water, and coral sand, is presented in Table 5. For comparison, the mix design proposed by Qin et al. (2023) [20] utilizes the same quantities of cement (450 kg) and coral sand, but adopts a lower water content of 225 kg, resulting in a W/C ratio of 0.50. Their mix aims to improve strength and reduce porosity, especially for use in marine environments. In contrast, the present study selects a slightly higher W/C ratio of 0.62 to account for the high water absorption of coral aggregate and to maintain sufficient workability for casting and compaction. The adopted mixture contains 450 kg of cement, 279 kg of water, and 754 kg of coral sand per cubic meter of concrete. This mix design is not fixed arbitrarily. Rather, it is established based on a systematic evaluation involving multiple trial batches and adjustments to key parameters, aiming to balance strength development, durability, and constructability. The process emphasizes achieving an optimized mix configuration suitable for structural applications in offshore and island environments where material performance and consistency are critical.

The necessary raw materials, including coral coarse aggregate, coral sand, cement, and water are measured precisely in accordance with the specified mix design. Then, the dry components are thoroughly mixed for a minimum of 5 minutes to ensure uniform distribution before the addition of water. Later on, water is gradually introduced into the dry mixture to initiate the hydration process until the fully mixed concrete exhibits a homogeneous texture, ensuring consistency before casting. The freshly cast specimens are submerged in water for curing to facilitate proper hydration and strength development. Finally, the dimensions of the cured specimens are measured to ensure they conform to the required standards

for subsequent mechanical testing. Coral concrete test specimens measuring 15×15×15 cm are prepared, fabricated, and cured in accordance with the guidelines outlined in standards [23, 24]. Fabrication process of the coral concrete test specimens is shown in Fig. 2.

(a) Preparation of materials

(b) Dry mixing process

(c) Addition of water into the mix

(d) Mixture after mixing

(e) Curing of test specimens

(f) Specimen dimension check

Fig. 2. Fabrication process of coral concrete test specimens

Table 5. Coral concrete mix proportions

Cement	Water	Coral sand	Coral coarse aggregates	Water to cement ratio
Current study				0.62
kg	kg	kg	kg	
450	279	754	745	
%	%	%	%	
20.20	12.52	33.84	33.44	
Qin et al (2023) [20]				0.50
kg	kg	kg	kg	
450	225	754	630	
%	%	%	%	
23.08	11.54	38.67	32.31	

2.3. Loading Device and Loading Method

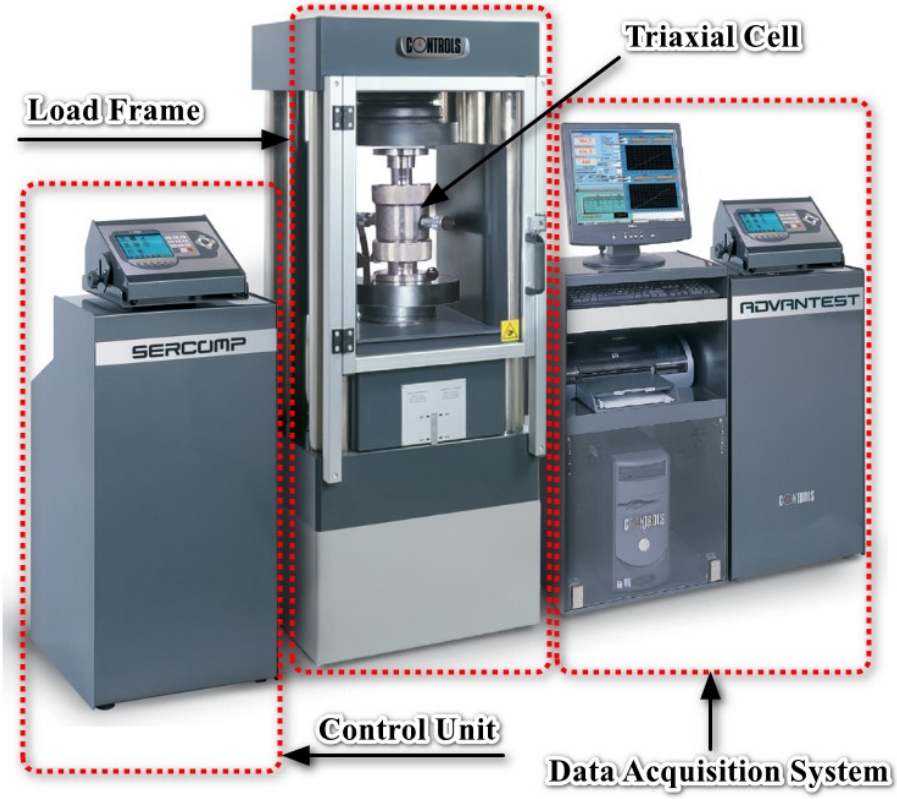

Fig. 3. Compression testing machine

The triaxial-uniaxial compression testing system of Controls Group is a specialized apparatus designed to evaluate the mechanical properties of rock specimens under controlled stress conditions, as shown in Fig. 3. This system typically consists of a triaxial cell, where the rock specimen is placed, a hydraulic actuator that applies axial load, and a confining pressure system that simulates in-situ stress conditions through hydraulic oil. The test setup also includes a pressure gauge to monitor applied stresses, a triaxial oil pump for regulating confining pressure, and a servo-controlled loading system to ensure precise application of force. Steel plates are used to transmit axial load, and a bleed hole enables controlled release of excess pressure. The entire

system is managed via a digital data acquisition and control unit, which records stress-strain behavior, failure characteristics, and deformation parameters. This configuration allows researchers to simulate complex geological conditions, providing valuable insights into material strength, deformation behavior, and failure mechanisms under compressive loading. The specimens are tested under a displacement-controlled mode, with a continuous loading rate of 0.2-0.6 MPa/s applied until failure.

For conventional concrete, the typical shape of the stress-strain curve is closely related to the mechanism of internal microcrack propagation, as illustrated in Fig. 4 [25-28]. Previous experimental studies have shown that cyclic loading and unloading do not significantly affect its behavior as long as the applied stress remains below approximately 50% of its compressive strength. However, a notable reduction in strength and stiffness is observed when the stress exceeds approximately 85% of its compressive strength [27, 29-32]. During each unloading and reloading cycle, a hysteresis loop is generated, with its area decreasing progressively with each successive cycle. Eventually, the material reaches failure due to fatigue. In this study, a total of 17 specimens, divided into several groups, are tested to evaluate the load-bearing capacity of coral concrete under cyclic compressive loading.

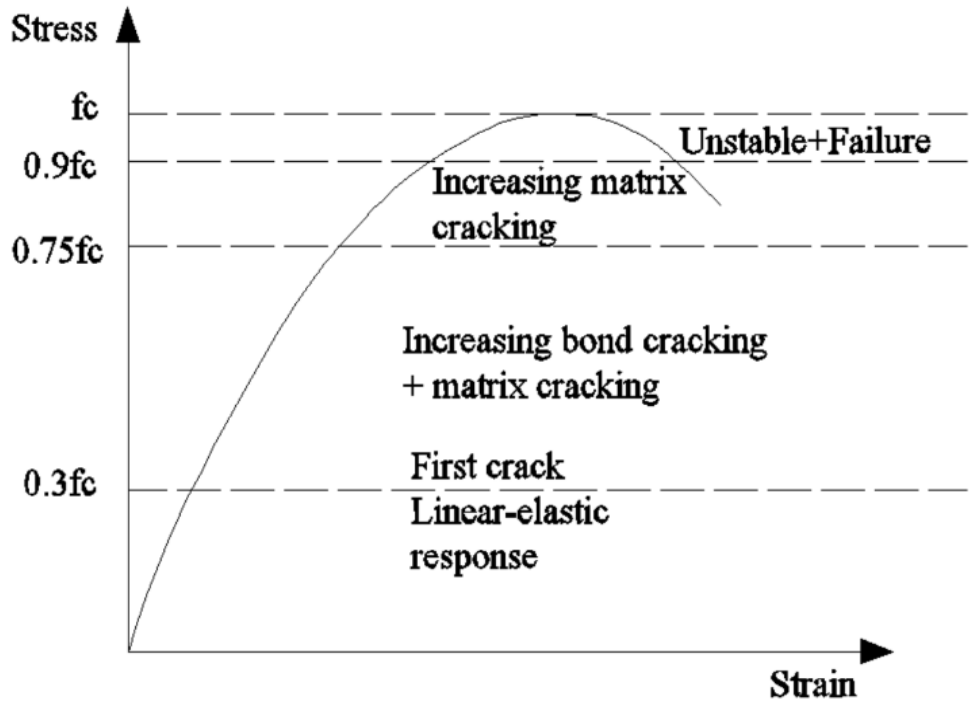

Fig. 4. Typical stress-strain curve for normal concrete under uniaxial loading

Table 6. Classification of test samples of coral concrete

Specimen group (G)	Specimen designation	Loading characteristics	Number of cycles
G1	S1, S2, S3	Without cyclic loading	NA
G2	S4, S5, S6	Repetitive loading at 30-60% of f_c	5
G3	S7, S8	Repetitive loading at 30-60% of f_c	10
G4	S9, S10	Repetitive loading at 30-60% of f_c	19
G5	S11, S12	Repetitive loading at 40-80% of f_c	5
G6	S13, S14	Repetitive loading at 40-80% of f_c	10
G7	S15, S16	Repetitive loading at 40-80% of f_c	19

Note: f_c (Maximum compressive strength)

Table 6 provides the classification of test samples used in this study, detailing the specimen grouping, loading characteristics, and number of loading cycles applied. Group G1 consists of control specimens denoted as S1, S2, and S3, which are tested without cyclic loading. Coral concrete specimens from groups G2 to G7, each subjected to different cyclic loading regimes. Specimens in groups G2, G3, and G4 are underwent repetitive loading at 30-60% of the maximum compressive strength, with 5, 10, and 19 loading cycles, respectively. Groups G5, G6, and G7 are subjected to higher cyclic loading levels at 40-80% of the maximum compressive strength, with 5, 10, and 19 cycles, respectively. The selection of 5, 10, and 19 loading cycles was intended to represent short-term, medium-term, and relatively long-term cyclic loading scenarios under marine conditions. Specifically, five cycles reflect the initial stage of repeated wave or tidal actions, ten cycles provide an intermediate stage to capture progressive degradation, and nineteen cycles were chosen to approximate extended exposure while still remaining within a manageable experimental framework. Although the number of cycles is limited compared to real-life service conditions, these values are sufficient to reveal key trends in stiffness degradation and strength reduction while maintaining experimental feasibility.

3. Result and discussion

3.1. Specimen damage analysis and Failure mechanism

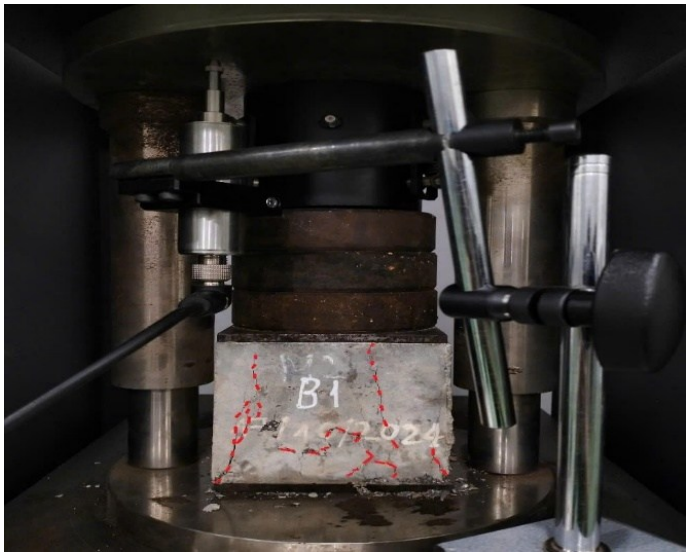

Fig. 5. Compression testing machine

Fig. 6. Destructive form of specimens in the Group G1

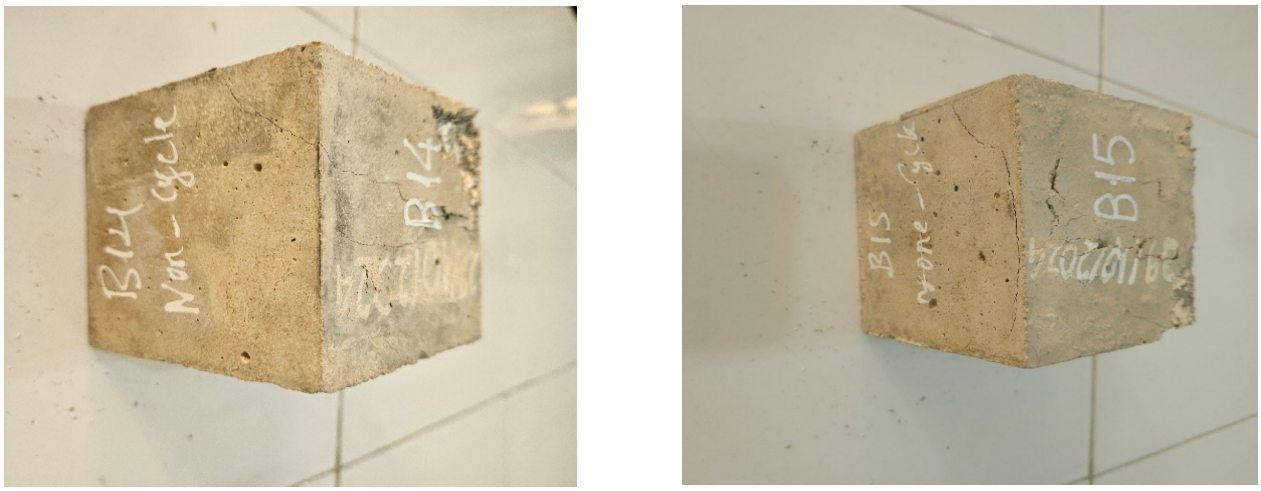

Fig. 6. (continued)

Fig. 7. Destructive form of specimens in the Group G2

Fig. 5 depicts a uniaxial compressive test conducted on a coral concrete specimen, using the triaxial-uniaxial compression testing system. The sample is placed vertically between two loading plates, with the top plate applying downward force while the bottom plate remains fixed. The machine is equipped with precision instruments, including a displacement or strain measurement system, to monitor deformation. Visible red-marked crack paths on the specimen indicate early stages of cracking due to applied axial stress. These cracks are predominantly vertical and diagonal, typical of concrete under compressive loading. As stress progresses, these cracks will likely propagate,

leading to eventual failure. The surrounding setup suggests careful control of test parameters, with the machine ensuring uniform load application and accurate data recording during the experiment.

Fig. 8. Destructive form of specimens in the Group G3

Fig. 9. Destructive form of specimens in the Group G4

Fig. 10. Destructive form of specimens in the Group G5

Figs. 6-12 show the destructive form of specimens of the specimens. The failure patterns observed in all sample groups exhibit several common characteristics under axial compressive

loading, as shown in Table 7. A primary similarity is the development of vertical or diagonal cracks along the height of the specimens, a failure mechanism typical of concrete under compressive stress [33-35]. These main cracks are primarily aligned along the loading axis and propagate as the stress increases, leading to structural separation. Additionally, surface deterioration is consistently observed across all groups, particularly in the form of localized surface spalling at the top and bottom regions where stress concentrations are highest. This spalling results from the detachment of small surface fragments due to high compressive forces. The propagation of main cracks follows a common trend, where vertical cracks gradually extend and interconnect, forming a network along the surface. Crack initiation frequently occurs at weak points, such as internal voids, specimen edges, and corners, indicating that internal material heterogeneity significantly influences the failure process.

Fig. 11. Destructive form of specimens in the Group G6

Fig. 12. Destructive form of specimens in the Group G7

Despite the overall similarities, differences in damage patterns and crack severity are observed across the various groups due to differences in loading conditions and the number of cycles. In Group G1, subjected to static loading, failure is characterized by relatively uniform vertical cracks with minimal branching or lateral propagation. Surface spalling is minimal, confined mainly to slight detachment at the top and bottom of the specimens. Groups G3 and G4, subjected to cyclic loading at 30-60% of the maximum compressive strength, show more complex cracking patterns.

Cracks in these groups extend diagonally and vertically, with branching becoming more prominent as the number of cycles increases. For instance, Group G4 (19 cycles) exhibits more severe and interconnected cracks compared to Group G3 (10 cycles), alongside greater surface spalling. In Groups G5 and G6, subjected to cyclic loading at 40-80% of maximum compressive strength, crack propagation is more extensive, with diagonal, horizontal, and vertical cracks forming a dense network. The spalling is more pronounced, with several sections of the concrete surface detaching, particularly at the top and bottom regions. The difference between Group G5 (5 cycles) and Group G6 (10 cycles) lies in the severity of cracking and spalling, with the latter showing wider and more interconnected cracks. The most severe damage is observed in Group G7, which undergoes cyclic loading at stress levels above 80% of the maximum compressive strength. This group displays dense and overlapping cracks that cover the entire surface of the specimens. Extensive fragmentation is evident, with large pieces of concrete detaching due to the high level of internal damage. The cracks in Group G7 penetrate deeply through the specimens, highlighting the severe structural degradation caused by prolonged high cyclic loading.

Table 7. Summary of differences in the damage pattern among groups

Specimen group (G)	Number of cycles	Main crack pattern	Surface spalling level	Crack propagation range
G1, G2	NA, 5 cycles	Predominantly vertical cracks	Minimal spalling, primarily at the top	Cracks propagate vertically with minimal branching
G3	10 cycles	Vertical and diagonal cracks	Localized spalling at the top and bottom	Cracks begin to show slight branching
G4	19 cycles	More distinct vertical and diagonal cracks	Increased spalling compared to G3	Wider crack distribution with interconnected branches
G5	5 cycles	Intermixed vertical and diagonal cracks	Moderate surface spalling	Cracks propagate moderately with lateral branches
G6	10 cycles	Extensive diagonal and horizontal cracks	Severe spalling across the surface	Cracks propagate throughout the surface, forming a network
G7	19 cycles	Dense and overlapping cracks	Large-scale spalling and fragmentation	Widespread damage with significant fragmentation

The initiation of microcracks in coral concrete primarily stems from the inherent heterogeneity of the material, particularly due to the unique microstructure of coral aggregates. The coral aggregates, being porous and relatively weak compared to conventional coarse aggregates, create localized stress concentrations under cyclic loading. As evident in the Fig. 13, these stress concentrations result in the early formation of microcracks at the interface between the coral aggregate and the surrounding cement paste, consistent with failure patterns described in some experimental studies [1, 2, 9, 10, 13, 36], where interfacial debonding precedes other forms of damage under compression. Under cyclic loading, the microcracks initially located at the interfacial transition zones propagate both radially and along aggregate boundaries, a behavior particularly visible in the images showing fragmented coral particles and extensive cracking along aggregate surfaces [1, 9, 36]. As cyclic loads are increased or sustained, these microcracks coalesce and

expand, bridging across aggregates and cement paste zones, leading to macrocrack formation that ultimately triggers structural failure. The crack morphology, ranging from thin, hairline fractures to wider cracks along weak zones, demonstrates progressive fatigue damage rather than immediate failure. Dense networks of microcracks around fractured coral particles indicate a mechanism of progressive aggregate breakage. As the coral aggregates fracture, internal voids are exposed, weakening the surrounding matrix and accelerating crack propagation, corresponding with findings from studies where cyclic loading induces significant cumulative damage by exploiting pre-existing flaws and weak interfaces. Compared to conventional concrete, the microcrack mechanism in coral concrete shows distinct characteristics due to the weak nature of coral aggregates, with cracks predominantly originating and propagating through the aggregates and interfacial zones rather than through the cement matrix. This explains the relatively brittle nature of failure observed in the specimens under cyclic conditions. In summary, the microcrack mechanisms observed in coral concrete under cyclic compression are characterized by early interfacial cracking, progressive aggregate breakage, and the formation of interconnected crack networks.

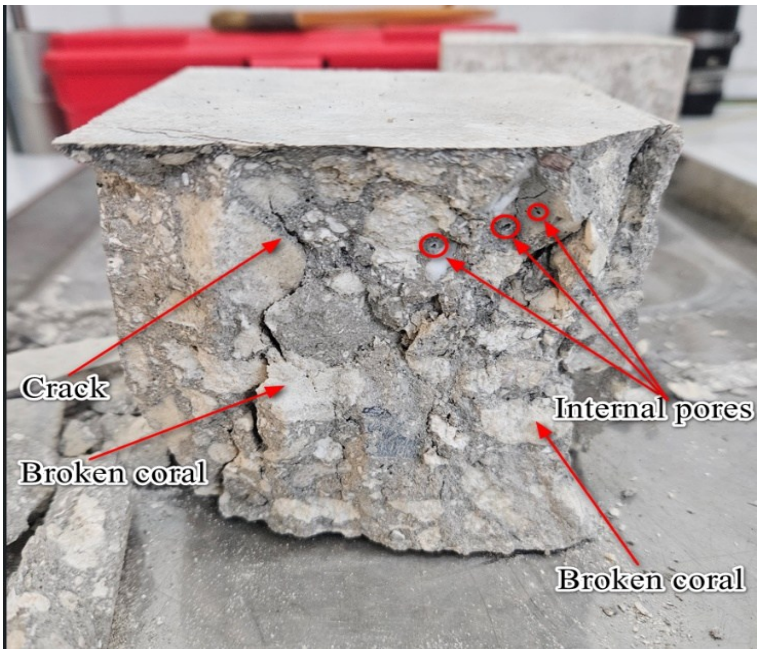

Fig. 13. Failure modes of coral concrete cube specimens under cyclic loading

3.2. Stress-strain curves

Fig. 14 shows the stress-strain curves coral concrete specimens under cyclic compressive loading. Overall, the stress–strain curves of coral concrete exhibited typical characteristics consistent with concrete behavior under cyclic loading. All stress–strain curves distinctly showed an initial linear elastic stage, followed by a nonlinear stage where distinct hysteresis loops emerged due to repetitive loading, culminating in stiffness degradation and a rapid increase in deformation upon reaching peak stress. Specimens in Group G1 (without cyclic loading) demonstrated typical characteristics of monotonic concrete loading curves, with clear curves, smaller deformation at peak stress, and relatively higher peak strengths. Specimens from Groups G2 to G7 (subjected to cyclic loading at stress ranges of 30–60% and 40–80%) exhibited reductions in compressive strength compared to those in Group G1, accompanied by inelastic hysteresis loops. Table 8 lists the maximum stress of test specimens. The observed reduction in maximum compressive stress for coral concrete specimens subjected to cyclic loading (Groups G2 to G7) compared to those without cyclic loading (Group G1) can be

explained through the microstructural damage mechanisms triggered by repetitive stress application. Moreover, the comparison between the control specimens (S1–S3) and the most severely affected cyclic loading group (S15–S16) reveals a significant reduction in average compressive strength of approximately 20%. Cyclic loading induces the early formation of microcracks, particularly at the interfacial transition zones between the porous coral aggregates and the surrounding cement paste [1, 9, 36]. Coral aggregates are inherently weaker and more porous compared to conventional aggregates, making them prone to localized stress concentrations under repetitive loading. These stress concentrations initiate microcracks early in the loading process, which propagate and coalesce as the number of cycles increases. This progressive damage weakens the material, reducing its ability to sustain higher compressive stresses. The cyclic application of loads at 30-60% or 40-80% of maximum compressive strength accelerates the deterioration of internal structural components. Each loading cycle incrementally contributes to the propagation of cracks, causing damage to the interfacial bond between the aggregates and the cement paste. As this damage accumulates, the material's overall stiffness and strength decrease, limiting the maximum compressive stress that the specimens can withstand. This behavior is consistent with fatigue phenomena in concrete materials, where repeated loading causes the progressive weakening of internal bonds [37-39]. As cyclic loading progresses, the coral aggregates begin to fracture due to their lower mechanical strength. The fractured aggregates further expose internal voids and weaken the surrounding matrix, leading to additional microcrack formation. The redistribution of stress around fractured aggregates further exacerbates damage in the interfacial zones. This degradation mechanism contrasts with specimens under non-cyclic loading (Group G1), where the absence of sustained cyclic stress allows the material to reach its inherent compressive strength before failure without experiencing the cumulative fatigue effects. In summary, the lower maximum compressive stress observed in cyclically loaded specimens is primarily due to the cumulative microcrack formation, interfacial debonding, aggregate fragmentation, and stress redistribution mechanisms that are activated under cyclic loading.

The stress–strain curve behaviors observed in the current study align well with findings reported in relevant literature, yet some differences are evident. In comparison with the experimental outcomes relating conventional concrete and recyled concrete [32, 40, 41], coral concrete exhibits a broader plastic deformation region and higher deformation capacity prior to failure, indicating enhanced ductility, which is largely attributed to the inherent porous structure and weaker coral aggregates. Meanwhile, research on normal concrete under cyclic compression of Andrawes [27] indicates an enhancement in the mechanical properties of concrete subjected to cyclic loading when conducted within a specific stress range (40% to 80% of the maximum compressive strength) and for a number of loading cycles ranging from 15 to 20. Furthermore, the experimental investigation conducted by Weichang et al. [42] on the effects of cyclic loading on rock and concrete highlighted a phenomenon, in which cyclic loading induced strain hardening in certain types of rock and concrete, temporarily resulting in increased compressive strength within a cyclic loading regime of under 100 cycles. In contrast, the coral concrete specimens in the present research exhibited no significant strengthening effect under cyclic loading conditions. Instead, the specimens consistently displayed stiffness degradation and reductions in maximum compressive stresses. Such behaviors of coral concrete, as described above, are predominantly attributed to its intrinsic porous microstructure and relatively weaker aggregate interfaces, which facilitate earlier

initiation and more rapid propagation of microcracks compared to conventional concrete. Thus, coral concrete under cyclic loading is generally more susceptible to fatigue deterioration rather than cyclic-induced strengthening, underscoring the necessity of material optimization or reinforcement to enhance long-term structural performance.

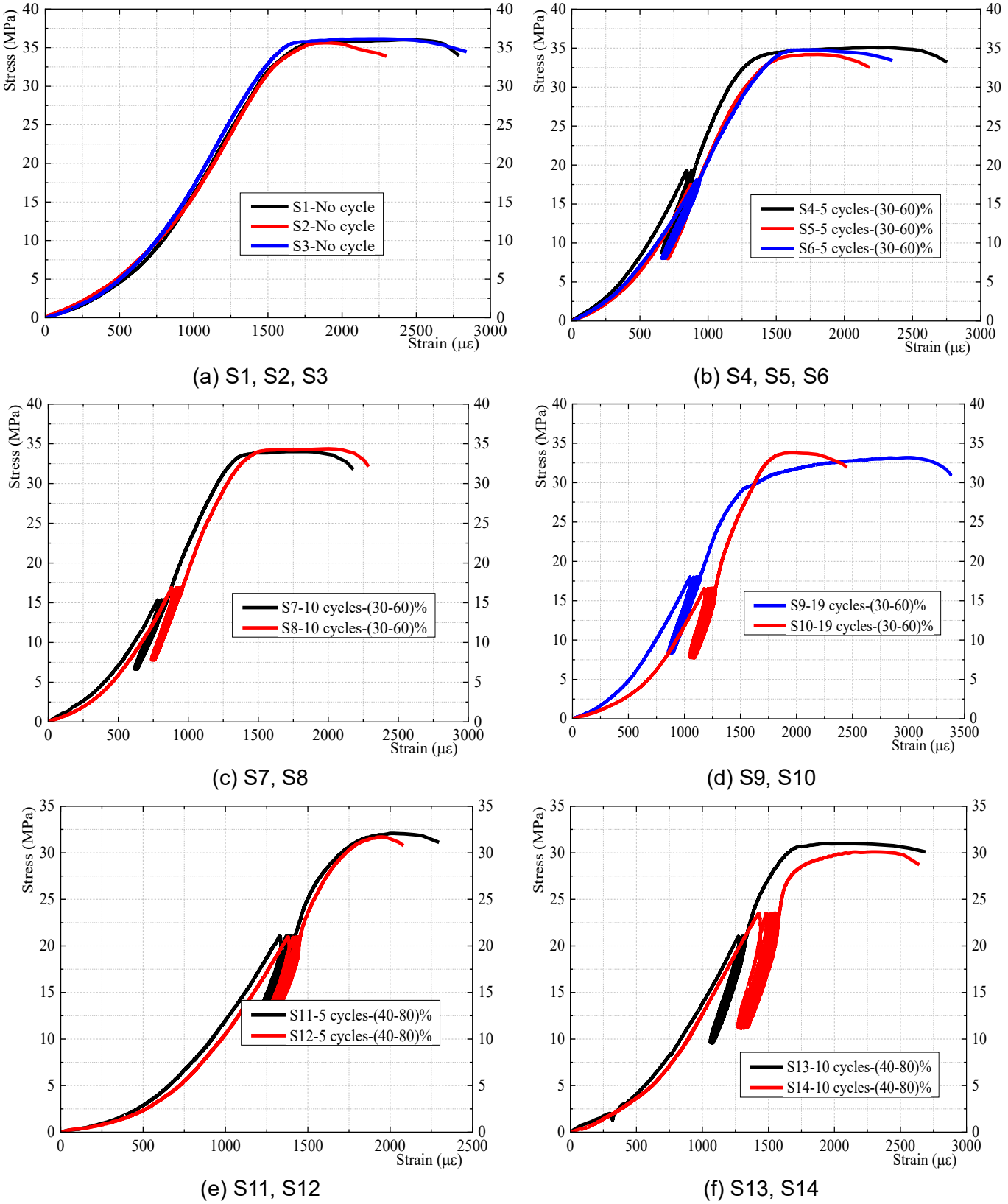

(a) S1, S2, S3

(b) S4, S5, S6

(c) S7, S8

(d) S9, S10

(e) S11, S12

(f) S13, S14

Fig. 14. Stress-strain curve of coral concrete specimens under cyclic compressive loading

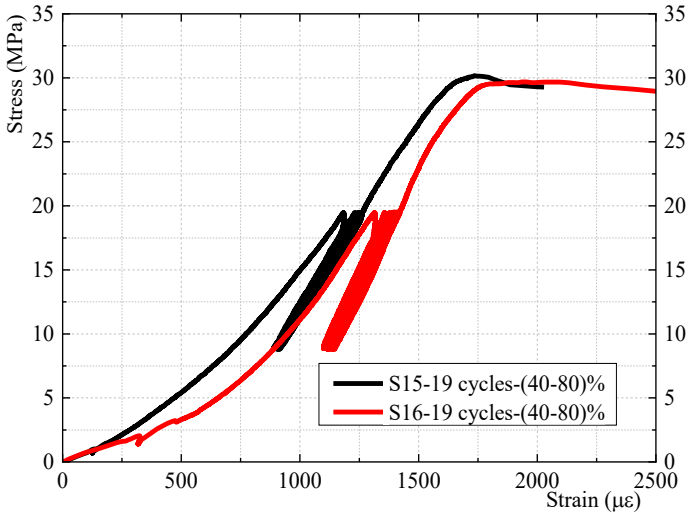

(g) S15, S16

Fig. 14. (continued)

Table 8. Maximum stress of test specimens

Specimen group (G)	Specimen designation	Loading characteristics	Maximum stress (MPa)
G1	S1/ S2/ S3	Without cyclic loading	36.0 / 35.7 / 36.15
G2	S4/ S5/ S6	Repetitive loading at 30-60% of maximum compressive strength-5 cycles	35.1/34.2/34.8
G3	S7/S8	Repetitive loading at 30-60% of maximum compressive strength-10 cycles	34.0/34.3
G4	S9/S10	Repetitive loading at 30-60% of maximum compressive strength-19 cycles	33.2/32.7
G5	S11/S12	Repetitive loading at 40-80% of maximum compressive strength-5 cycles	32.1/31.7
G6	S13/S14	Repetitive loading at 40-80% of maximum compressive strength-10 cycles	30.9/30.1
G7	S15/S16	Repetitive loading at 40-80% of maximum compressive strength-19 cycles	30.2/29.7

3.3. The modulus of elasticity

The elastic modulus of concrete is a fundamental mechanical property that characterizes its stiffness and deformation behavior under loading. Various methods have been developed to determine, each with distinct advantages and applications depending on material behavior and testing conditions. The tangent modulus method is commonly used for evaluating the instantaneous stiffness of concrete at a specific point on the stress-strain curve, typically at the origin or near a predefined stress level (ACI 318; ASTM C469) [43, 44]. For materials subjected to cyclic or repeated loading, where stiffness degradation occurs, more advanced techniques such as the Least Squares Regression Method (LSRM) is applied. Unlike conventional two-point methods, which rely on selecting specific stress-strain pairs, the least squares method minimizes the impact of experimental noise and variability by fitting a linear trend to the elastic portion of the stress-strain curve. This approach is particularly advantageous for materials exhibiting non-ideal elasticity, such as concrete under cyclic

loading, where microcrack formation and stiffness degradation lead to deviations from purely linear behavior. Numerous studies have employed Least Squares Regression Method to determine the secant modulus of concrete [27, 45-48]. The LSRM is an effective approach for determining the secant modulus of concrete based on the stress-strain response. This method involves selecting an appropriate strain interval, typically ranging from 0.1% to 50% of the peak stress, to define the linear approximation. In instances where the initial stage of the stress-strain curve exhibits instability and nonlinear behavior, it is excluded from the analysis. Then, the stress-strain relationship is assumed to follow a linear trend, expressed as:

$$\sigma = E_s.\varepsilon + C \quad (1)$$

where: σ is the stress (MPa), ε is the strain (με);

E_s is the secant modulus (MPa), and C is the intercept.

The least squares regression technique is then applied to minimize the sum of squared residuals, yielding the best-fit linear approximation. The modulus is computed as:

$$E_s = \frac{\sum\left(\varepsilon_i - \bar{\varepsilon}\right)\left(\sigma_i - \bar{\sigma}\right)}{\sum\left(\varepsilon_i - \bar{\varepsilon}\right)^2} \quad (2)$$

where: ε_i, σ_i and are the individual strain and stress values; $\bar{\varepsilon}, \bar{\sigma}$ are the mean strain and stress.

The secant modulus results of the coral concrete specimens are presented in Fig. 15 and Table 9. Specimens without cyclic loading (Group G1: S1–S3) exhibit the highest secant modulus values, ranging from 23625 MPa to 24473 MPa, indicating a relatively stiff elastic response. These values serve as a baseline for evaluating the degradation effect caused by cyclic loading. As both the number of cycles and the amplitude of loading increase, a consistent and gradual reduction in the secant modulus is observed across all other specimen groups. Specifically, for specimens subjected to cyclic loading at 30–60% of maximum compressive strength, the secant modulus declines from approximately 22521 MPa (G2: 5 cycles) to 21168 MPa (G4: 19 cycles). In the 40–80% stress range, a more significant reduction is evident, with modulus values decreasing from 20718 MPa (G5: 5 cycles) to 18824 MPa (G7: 19 cycles). The largest observed reduction in secant modulus occurs between G1 and G7. When comparing the minimum value in G7 (18824 MPa) to the maximum in G1 (24473 MPa), the modulus decreases by approximately 5649 MPa, corresponding to a reduction of about 23.1%. This decline highlights the detrimental impact of repeated high-stress cyclic loading on the elastic stiffness of coral concrete. The progressive reduction can be attributed to microstructural damage accumulation, increased internal cracking, and deterioration of the coral aggregate–cement paste interface. The results confirm that both loading amplitude and number of cycles significantly influence the degradation of stiffness. Notably, modulus loss is more pronounced under higher stress ranges (40–80%), reflecting the activation of more severe damage mechanisms at elevated cyclic stress levels. Furthermore, although slight variations are observed between specimens within the same group (e.g., S4/S5/S6 or S15/S16), the regression-based slope fitting method applied within the elastic region consistently yields R^2 values above 0.97. This consistency supports the validity and reliability of the linear approximation in estimating the secant modulus.

The static elastic modulus (E_c) of coral concrete, as summarized in Table 10, demonstrates notable consistency across multiple studies with the same compressive strength. In the current study, the E_c values for cubic specimens with a compressive strength of 36.0, 35.7, and 36.15 MPa range from 23940 MPa to 24473 MPa, indicating relatively high stiffness of the material. These values align closely with the findings of Yang et al. [49, 50], who report E_c values of 24500 MPa and 23000 MPa for coral concrete with compressive strengths of 36.8 MPa and 36.29 MPa, respectively. This suggests that, within a

similar strength range, coral concrete exhibits comparable elastic performance regardless of the specific research conditions or material origins. Moreover, Wang et al. [51] report a slightly higher E_c value of 28800 MPa corresponding to a compressive strength of 37.73 MPa, which exceeds the values found in other studies. This discrepancy may result from differences in the microstructure, mix proportions, or curing regimes applied in their research. The data imply a general trend in which E_c increases/decreases with compressive strength, as expected in conventional concrete, but the correlation is not strictly linear, especially for coral concrete, where porosity and aggregate-matrix bonding play significant roles in determining stiffness. Furthermore, the average static elastic modulus obtained in the present study (24 GPa) accounts for approximately 69.3% to 76% of the corresponding value for conventional concrete of the same strength grade, as calculated based on the CEB-FIP 1990, and AIJ 1985 [52-54]. While the elastic modulus of coral concrete is generally lower than that of normal concrete with equivalent strength (due to its porous structure and weaker aggregate interlock), it remains within a functional range suitable for structural applications in marine environments.

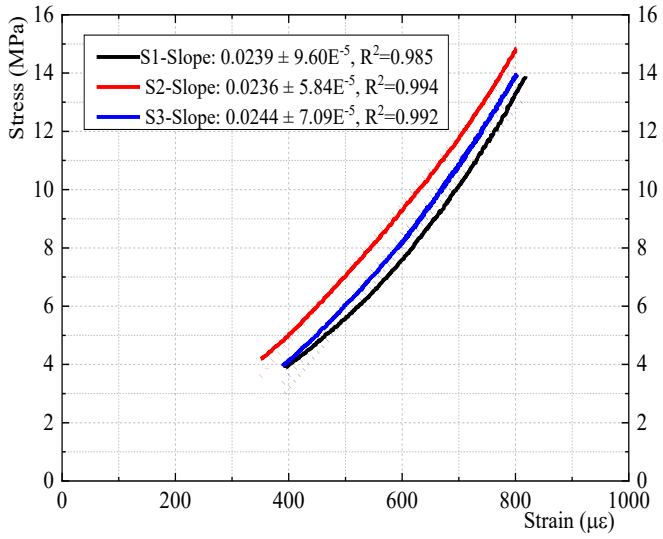

(a) S1, S2, S3

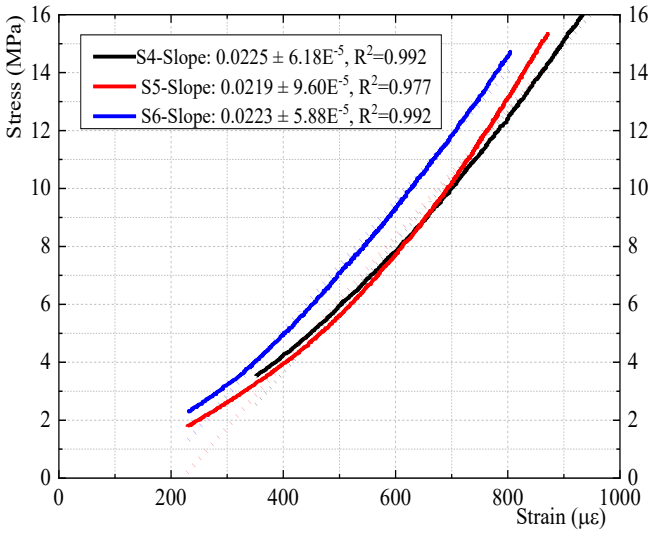

(b) S4, S5, S6

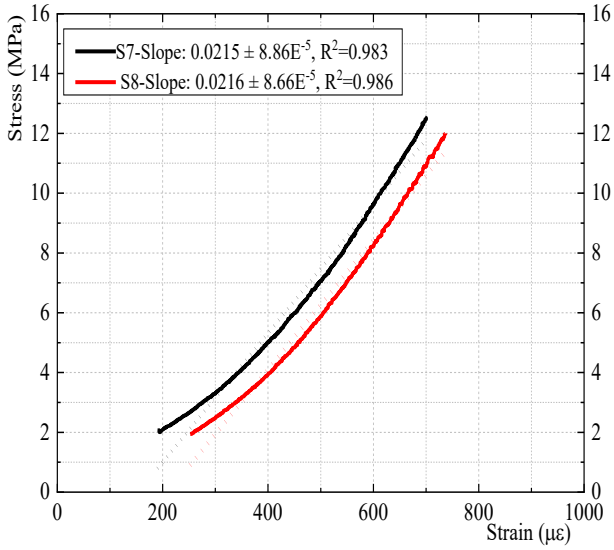

(c) S7, S8

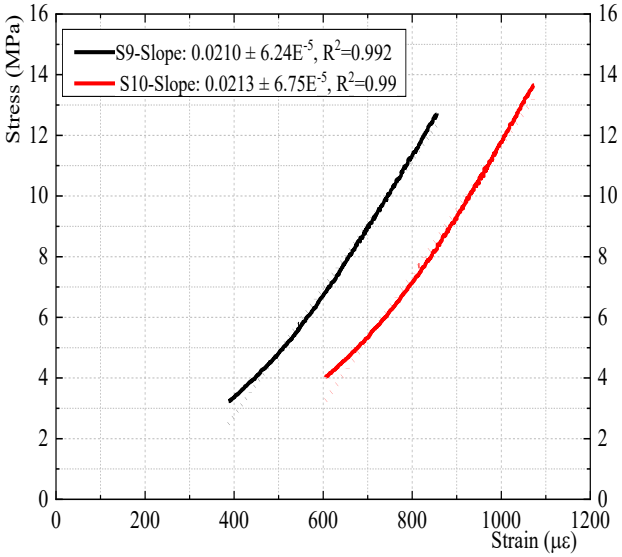

(d) S9, S10

Fig. 15. Secant modulus of specimens

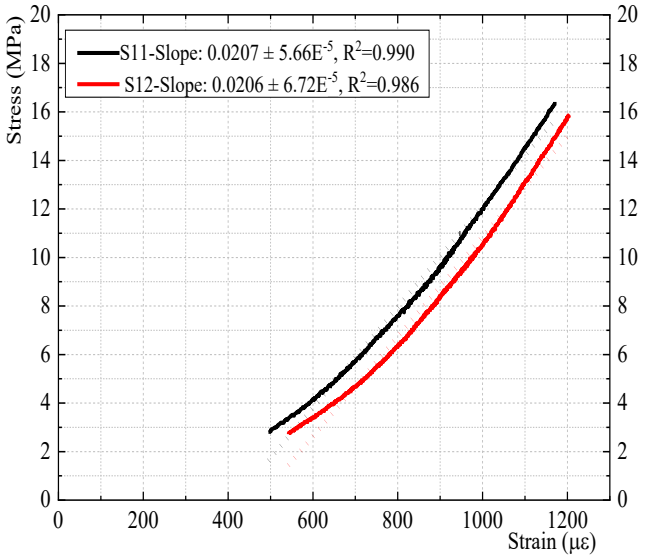

(e) S11, S12

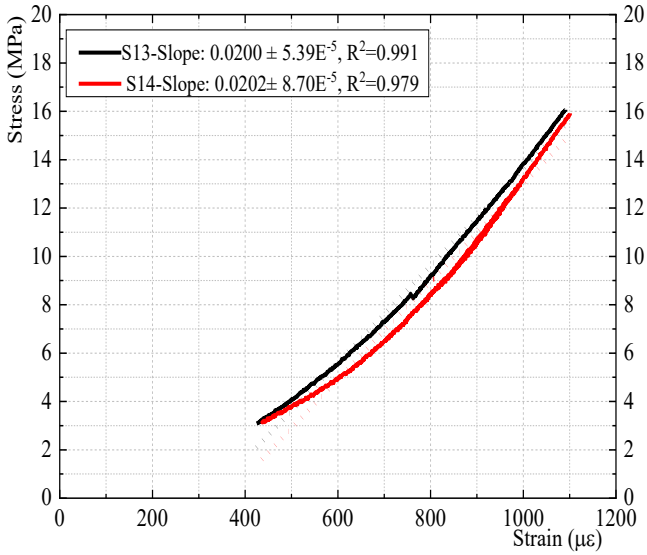

(f) S13, S14

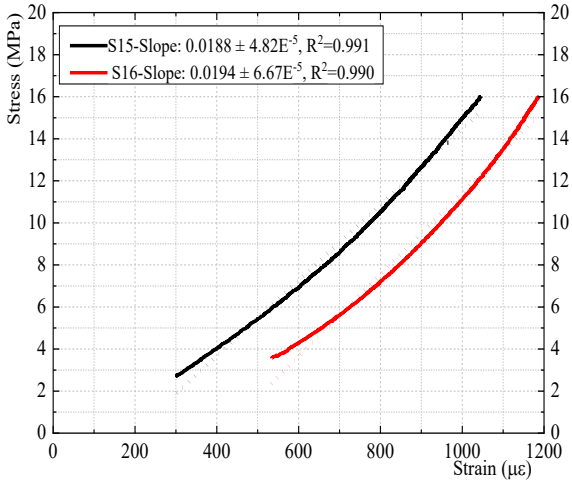

(g) S15, S16

Fig. 15. (continued)

Table 9. Secant modulus value of the specimens

Specimen group (G)	Specimen designation	Loading characteristics	Secant modulus (MPa)
G1	S1/ S2/ S3	Without cyclic loading	23940/ 23625 / 24473
G2	S4/ S5/ S6	Repetitive loading at 30-60% of maximum compressive strength-5 cycle	22521/21933/22365
G3	S7/S8	Repetitive loading at 30-60% of maximum compressive strength-10 cycles	21585/21625
G4	S9/S10	Repetitive loading at 30-60% of maximum compressive strength-19 cycles	21168/21392
G5	S11/S12	Repetitive loading at 40-80% of maximum compressive strength-5 cycles	20718/20654
G6	S13/S14	Repetitive loading at 40-80% of maximum compressive strength-10 cycles	20017/20267
G7	S15/S16	Repetitive loading at 40-80% of maximum compressive strength-19 cycles	18824/19415

Table 10. Static elastic modulus (E_c) of coral concrete as reported in various studies

Sources	Cubic specimens (mm)	Compressive strength	E_c (MPa)
Current study	150×150×150	36.0 / 35.7 / 36.15	23940/ 23625 / 24473
Yang et al. (2019) [49]	150×150×150	36.8	24500
Yang et al. (2018) [50]	150×150×150	36.29	23000
Wang et al. [51]	150×150×150	37.73	28800

4. Conclusions

This experimental study investigates the mechanical properties and cyclic compression behavior of coral concrete, with a focus on strength degradation, stress-strain characteristics, and failure mechanisms. Based on the results obtained from a series of controlled cyclic loading tests, the following conclusions are drawn:

Unlike conventional concrete, coral concrete exhibits early fatigue-induced deterioration and rapid stiffness degradation beginning from the initial loading cycles. This behavior is primarily attributed to the porous microstructure of coral aggregates and the weaker bond strength at the aggregate–paste interface. The deformation under cyclic loading is significantly higher than that of normal concrete, indicating reduced resistance to fatigue-induced damage.

The experimental results reveal clear hysteresis loops in the stress–strain curves, confirming the accumulation of internal damage with increasing loading cycles. Microcrack initiation and propagation predominantly occur at the interfacial transition zones, eventually leading to coalescence and macrocrack formation. These observations are supported by both visual inspection of failed specimens and the progressive decline in secant modulus values across all cyclic loading groups.

The secant modulus of coral concrete shows a marked decline with increasing cycle number and loading amplitude. Specifically, a maximum reduction of approximately 23.1% in modulus is observed between the control group and specimens subjected to 19 cycles at 40–80% of peak compressive strength. Simultaneously, the average compressive strength also decreases by approximately 20%, confirming the dual impact of cyclic loading on both stiffness and strength. Notably, the average static elastic modulus (24 GPa) measured in this study accounts for only 69.3% to 76% of the corresponding values for conventional concrete of the same strength grade, as predicted by design codes such as CEB-FIP 1990, and AIJ 1985.

In contrast to conventional concrete, which has been shown in previous studies to exhibit slight improvements in compressive strength and stiffness under low-cycle cyclic loading (typically fewer than 100 cycles), coral concrete demonstrates an opposite trend. Even under fewer than 20 loading cycles, both the strength and secant modulus of coral concrete show the degradation. Accordingly, structural design for marine applications using coral concrete should incorporate greater safety factors to account for its increased vulnerability under cyclic loading.

Failure patterns under monotonic and cyclic compression differ noticeably. While control specimens generally exhibit typical vertical splitting and conical shear failure, those subjected to repeated loading display more complex cracking networks, earlier onset of damage, and surface fragmentation. These behaviors indicate that cyclic loading not only reduces strength and stiffness but also alters the fracture mode of coral concrete.

Future work

Future research will expand the experimental program to optimize coral concrete mixtures under a greater number of cyclic loading cycles and to examine the effect of fiber incorporation on the performance of coral concrete.

Acknowledgement

This research is funded by Le Quy Don

Technical University Research Fund under the grand number "25.01.56".

References

[1] C. Wang, L. Sun, C. Zhang, C. Li, P. Qiao, X. Chen. (2024). Experimental study on the mechanical properties and uniaxial compressive constitutive relationship of sea sand coral concrete. *Journal of Building Engineering*, 87, 109062. https://doi.org/10.1016/j.jobe.2024.109062

[2] L. Rao, L. Wang, Y. Zheng. (2022). Experimental research on mechanical properties and compression constitutive relationship of PVA fiber-reinforced coral concrete. *Materials*, 15(5), 1762. https://doi.org/10.3390/ma15051762

[3] M.E. Portman. (2019). Detached islands: Artificial islands as adaptation challenges in the making. *DIE ERDE – Journal of the Geographical Society of Berlin*, 150(3), 158–168. https://doi.org/10.12854/erde-2019-430

[4] Y.-N. Wang, J.-R. Peng, C. Bogireddy, B. Rattan, M.-X. Tan. (2024). Artificial islands in modern development: Construction, applications, and environmental challenges. *Marine Georesources & Geotechnology*, 42(12), 1896–1906. https://doi.org/10.1080/1064119X.2023.2295034

[5] J. Babinard, C.R. Bennett, M.E. Hatziolos, A. Faiz, A. Somani. (2014). Sustainably managing natural resources and the need for construction materials in Pacific island countries: The example of South Tarawa, Kiribati. *Natural Resources Forum*, 38(1), 58–66. https://doi.org/10.1111/1477-8947.12035

[6] L. Zhou, S. Guo, Z. Zhang, C. Shi, Z. Jin, D. Zhu. (2021). Mechanical behavior and durability of coral aggregate concrete and bonding performance with fiber-reinforced polymer (FRP) bars: A critical review. *Journal of Cleaner Production*, 289, 125652. https://doi.org/10.1016/j.jclepro.2020.125652

[7] L. Zhang, D. Niu, B. Wen, Q. Fu, Y. Zhang. (2021). Corrosion rate models of reinforcement in modified coral aggregate concrete. *Construction and Building Materials*, 288, 123099.https://doi.org/10.1016/j.conbuildmat.2021.123099

[8] Y. Chu, A. Wang, Y. Zhu, H. Wang, K. Liu, R. Ma, L. Guo, D. Sun. (2021). Enhancing the performance of basic magnesium sulfate cement-based coral aggregate concrete through gradient composite design technology. *Composites Part B: Engineering*, 227, 109382. https://doi.org/10.1016/j.compositesb.2021.109382

[9] B. Da, H. Huang, T. Tao, Y. Chen, D. Chen. (2024). Experimental and numerical investigations on the mechanical properties of coral aggregate seawater concrete. *Engineering Fracture Mechanics*, 310, 110498. https://doi.org/10.1016/j.engfracmech.2024.110498

[10] Y. Huang, X. Li, Y. Lu, H. Wang, Q. Wang, H. Sun, D. Li. (2019). Effect of mix component on the mechanical properties of coral concrete under axial compression. *Construction and Building Materials*, 223, 736–754. https://doi.org/10.1016/j.conbuildmat.2019.07.015

[11] L. Ma, Z. Li, J. Liu, L. Duan, J. Wu. (2019). Mechanical properties of coral concrete subjected to uniaxial dynamic compression. *Construction and Building Materials*, 199, 244–255.https://doi.org/10.1016/j.conbuildmat.2018.12.032

[12] H. Wang, L. Wang, L. Li, B. Cheng, Y. Zhang, Y. Wei. (2020). The study on the whole stress–strain curves of coral fly ash-slag alkali-activated concrete under uniaxial compression. *Materials*, 13(19), 4291. https://doi.org/10.3390/ma13194291

[13] H. Shi, L. Mo, M. Pan, L. Liu, Z. Chen. (2022). Experimental study on triaxial compressive mechanical properties of polypropylene fiber coral seawater concrete. *Materials*, 15(12), 4234.

https://doi.org/10.3390/ma15124234

[14] Z. Chen, Y. Liang, Q. Qin, F. Ning, Y. Liang. (2025). Mechanical properties and constitutive model of sisal fiber coral seawater concrete under uniaxial cyclic compression. *Journal of Building Engineering*, 100, 111646. https://doi.org/10.1016/j.jobe.2024.111646

[15] D. Vu, P. Stroeven, V. Bui. (2001). Strength and durability aspects of calcined kaolin-blended Portland cement mortar and concrete. *Cement and Concrete Composites*, 23(6), 471–478. https://doi.org/10.1016/S0958-9465(00)00091-3

[16] H.-D. Do, V.-N. Pham, H.-H. Nguyen, P.-N. Huynh, J. Han. (2021). Prediction of unconfined compressive strength and flexural strength of cement-stabilized sandy soils: a case study in Vietnam. *Geological Engineering*, 39, 4947–4962. https://doi.org/10.1007/s10706-021-01805-z

[17] N.D. Chau, K. Wątor, P. Rusiniak, Z. Gorczyca, D.V. Hao. (2022). Chemical composition, radioactive and stable isotopes in several selected thermal waters in North Vietnam. *Ecological Indicators*, 138, 108856. https://doi.org/10.1016/j.ecolind.2022.108856

[18] C.T.T. Trang, D.C. Thung, L.V. Nam, P.T. Kha, N.V. Bach, D.H. Ngoc. (2020). Assessment of Sea Water Quality in some Limestone Island and Archipelagos areas, Viet Nam. *Journal of Science: Earth Environmental Sciences*, 36(1), 70-78. https://doi.org/10.25073/2588-1094/vnuees.4556

[19] ASTM C33/C33M-18. (2018). Standard Specification for Concrete Aggregates. American Society for Testing and Materials, West Conshohocken, PA, USA.

[20] Q. Qin, Q. Meng, M. Gan, Z. Ma, Y. Zheng. (2023). Deterioration mechanism of coral reef sand concrete under scouring and abrasion environment and its performance modulation. *Construction and Building Materials*, 408, 133607.https://doi.org/10.1016/j.conbuildmat.2023.133607

[21] J. Li, Y. Xu, Z. Tian, J. Ma, P. Jing, Z. Song. (2021). Study on leaching damage mechanism of calcium ions of reactive powder concrete (RPC) under ion corrosion. *Construction and Building Materials*, 269, 121303. https://doi.org/10.1016/j.conbuildmat.2020.121303

[22] W. Kushartomo, H. Wiyanto, D. Christianto. (2022). Effect of Cement–Water Ratio on the Mechanical Properties of Reactive Powder Concrete with Marble Powder as Constituent Materials. *In: Lie, H.A., Sutrisna, M., Prasetijo, J., Hadikusumo, B.H., Putranto, L.S. (eds) Proceedings of the Second International Conference of Construction, Infrastructure, and Materials. Lecture Notes in Civil Engineering, vol 216. Springer, Singapore*. https://doi.org/10.1007/978-981-16-7949-0_16

[23] Ministry of Science and Technology. (2022). TCVN 3105:2022. Fresh and hardened concrete – Sampling, making and curing of test specimens (Vietnamese Standard).

[24] European Committee for Standardization. (2012). EN 125.690-1:2012. Testing hardened concrete – Part 1: Shape, dimensions and other requirements for specimens and moulds.

[25] A.K. Samani, M.M. Attard. (2012). A stress–strain model for uniaxial and confined concrete under compression. *Engineering Structures*, 41, 335–349. https://doi.org/10.1016/j.engstruct.2012.03.027

[26] J.C. Lim, T. Ozbakkaloglu. (2014). Stress–strain model for normal- and light-weight concretes under uniaxial and triaxial compression. *Construction and Building Materials*, 71, 492–509. https://doi.org/10.1016/j.conbuildmat.2014.08.050

[27] G.M. Andrawes. (2014). The cyclic loading of normal concrete in a specific stress range. *Jordan Journal of Civil Engineering*, 8(3), 271-281.

[28] S.H. Ahmad, S.P. Shah. (1982). Complete triaxial stress–strain curves for concrete.

Journal of the Structural Division, 108(4), 728–742. https://doi.org/10.1061/JSDEAG.0005921

[29] B.P. Sinha, K.H. Gerstle, L.G. Tulin. (1964). Stress-strain relations for concrete under cyclic loading. *Journal Proceedings*, 61(2) 195–212. DOI: 10.14359/7775

[30] W.-P. Kwan, S.L. Billington. (2001). Simulation of structural concrete under cyclic load. *Journal of Structural Engineering*, 127(12), 1391–1401. https://doi.org/10.1061/(ASCE)0733-9445(2001)127:12(1391)

[31] B.Y. Bahn, C.-T.T. Hsu. (1998). Stress-strain behavior of concrete under cyclic loading. *Materials Journal*, 95(2), 178–193. DOI: 10.14359/363

[32] F. Aslani, R. Jowkarmeimandi. (2012). Stress–strain model for concrete under cyclic loading. *Magazine of Concrete Research*, 64(8), 673–685. http://dx.doi.org/10.1680/macr.11.00120

[33] Z. Yu, Q. Huang, X. Xie, N. Xiao. (2018). Experimental study and failure criterion analysis of plain concrete under combined compression-shear stress. *Construction and Building Materials*, 179, 198–206. https://doi.org/10.1016/j.conbuildmat.2018.05.242

[34] J.G.M. van Mier. (2014). Failure of concrete under uniaxial compression: An overview. *Fracture Mechanics of Concrete Structures*, 2, 1169–1182.

[35] B. Mu, K.V. Subramaniam, S.P. Shah. (2004). Failure mechanism of concrete under fatigue compressive load. *Journal of Materials in Civil Engineering*, 16(6), 566–572. DOI: 10.1061/(ASCE)0899-1561(2004)16:6(566)

[36] B. Zhang, H. Zhu, F. Li, Z. Dong, P. Zhang. (2021). Compressive stress-strain behavior of seawater coral aggregate concrete incorporating eco-efficient alkali-activated slag materials. *Construction and Building Materials*, 299, 123886. https://doi.org/10.1016/j.conbuildmat.2021.123886

[37] I.N. Yadav, K.B. Thapa. (2020). Fatigue damage model of concrete materials. *Theoretical and Applied Fracture Mechanics*, 108, 102578. https://doi.org/10.1016/j.tafmec.2020.102578

[38] R.L. Riyar, Mansi, S. Bhowmik. (2023). Fatigue behaviour of plain and reinforced concrete: A systematic review. *Theoretical and Applied Fracture Mechanics*, 125, 103867. https://doi.org/10.1016/j.tafmec.2023.103867

[39] F.Z. Kachkouch, C.C. Noberto, L.F.d.A.L. Babadopulos, A.R.S. Melo, A.M.L. Machado, N. Sebaibi, F. Boukhelf, Y. El Mendili. (2022). Fatigue behavior of concrete: A literature review on the main relevant parameters. *Construction and Building Materials*, 338, 127510. https://doi.org/10.1016/j.conbuildmat.2022.127510

[40] A. Saboori, S. Yazdani, D. Tolliver. (2015). Anisotropic damage mechanics modeling of concrete under biaxial fatigue loading. *Open Journal of Civil Engineering*, 5(1), 8-16. http://dx.doi.org/10.4236/ojce.2015.51002

[41] X. Hu, Q. Lu, Z. Xu, W. Zhang, S. Cheng. (2018). Compressive stress-strain relation of recycled aggregate concrete under cyclic loading. *Construction and Building Materials*, 193, 72–83. https://doi.org/10.1016/j.conbuildmat.2018.10.137

[42] C. Weichang, L. Shouding, L. Li, S. Mingshen. (2020). Strengthening effects of cyclic load on rock and concrete based on experimental study. *International Journal of Rock Mechanics and Mining Sciences*, 135, 104479.https://doi.org/10.1016/j.ijrmms.2020.104479

[43] ASTM. (2010). Standard Test Method for Static Modulus of Elasticity and Poisson's Ratio of Concrete in Compression, C469-02. West Conshohocken, PA, USA.

[44] ACI 318-19. (2022). Building Code Requirements for Structural Concrete and

Commentary. American Concrete Institute, Farmington Hills, MI.

[45] A. Czajkowska, W. Raczkiewicz, M. Ingaldi. (2023). Determination of the linear correlation coefficient between Young's modulus and the compressive strength in fibre-reinforced concrete based on experimental studies. *Production Engineering Archives*, 29(3), 288–297. DOI: 10.30657/pea.2023.29.33

[46] B. Özkul, A.D. Karaoğlan. (2011). Regression control chart for determination of Young's modulus: A case study. *Scientific Research and Essays*, 6(30), 6393-6403. DOI: 10.5897/SRE11.1800

[47] M.F.M. Zain, S.M. Abd, K. Sopian, M. Jamil, A.I. Che-Ani. (2008). Mathematical regression model for the prediction of concrete strength. *Proceedings of the 10th WSEAS International Conference on Mathematical Methods, Computational Techniques and Intelligent Systems, 396-402*.

[48] C. Zhang, P. Liu, T. Song, B. He, W. Li, Y. Peng. (2024). Elastic Modulus Prediction of Ultra-High-Performance Concrete with Different Machine Learning Models. *Buildings*, 14(10), 3184. https://doi.org/10.3390/buildings14103184

[49] S. Yang, X. Zhang, M. Yu, J. Yao. (2019). An analytical approach to predict fracture parameters of coral aggregate concrete immersed in seawater. *Ocean Engineering*, 191, 106508. https://doi.org/10.1016/j.oceaneng.2019.106508

[50] S. Yang, C. Yang, M. Huang, Y. Liu, J. Jiang, G. Fan. (2018). Study on bond performance between FRP bars and seawater coral aggregate concrete. *Construction and Building Materials*, 173, 272–288. https://doi.org/10.1016/j.conbuildmat.2018.04.015

[51] L. Wang, N. Shen, M. Zhang, F. Fu, K. Qian. (2020). Bond performance of Steel-CFRP bar reinforced coral concrete beams. *Construction and Building Materials*, 245, 118456. https://doi.org/10.1016/j.conbuildmat.2020.118456

[52] CEB-FIP. (1993). Model code 1990: Design code. *Thomas Telford Publishing*.

[53] Architectural Institute of Japan. (1985). Standard for structural calculation of reinforced concrete structures, Chapter 2, 8-11. AIJ, Japan.

[54] N. Dawood, H. Marzouk. (2010). Reinforced concrete panels subjected to uniaxial and biaxial tension. *Journal of Advanced Concrete Technology*, 8(1), 59–73. https://doi.org/10.3151/jact.8.59